Visualizing Atomic-Scale Negative Differential Resistance in Bilayer Graphene

Keun Su Kim,[1] Tae-Hwan Kim,[2] Andrew L. Walter,[1,3] Thomas Seyller,[4] Han Woong Yeom,[2,*]
Eli Rotenberg,[1] and Aaron Bostwick[1,†]

[1]*Advanced Light Source, E. O. Lawrence Berkeley National Laboratory, Berkeley, California 94720, USA*
[2]*Center for Low Dimensional Electronic Symmetry and Department of Physics, Pohang University of Science and Technology,
Pohang 790-784, Korea*
[3]*Department of Molecular Physics, Fritz-Haber-Institut der Max-Planck-Gesellschaft, Faradayweg 4-6, 14195 Berlin, Germany*
[4]*Lehrstuhl für Technische Physik, Universität Erlangen-Nürnberg, Erwin-Rommel-Strasse 1, 91058 Erlangen, Germany*
(Received 16 August 2012; published 18 January 2013)

We investigate the atomic-scale tunneling characteristics of bilayer graphene on silicon carbide using the scanning tunneling microscopy. The high-resolution tunneling spectroscopy reveals an unexpected negative differential resistance (NDR) at the Dirac energy, which spatially varies within the single unit cell of bilayer graphene. The origin of NDR is explained by two near-gap van Hove singularities emerging in the electronic spectrum of bilayer graphene under a transverse electric field, which are strongly localized on two sublattices in different layers. Furthermore, defects near the tunneling contact are found to strongly impact on NDR through the electron interference. Our result provides an atomic-level understanding of quantum tunneling in bilayer graphene, and constitutes a useful step towards graphene-based tunneling devices.

Understanding quantum tunneling at the atomic level is essential in the study of nanoscale materials and their applications in the tunneling devices [1,2]. One of the most interesting tunneling phenomena is negative differential resistance (NDR), characterized by the reversal of the standard current-voltage relationship, decreasing current with increasing voltage. NDR is the basic operating principle of Esaki and resonant-tunneling diodes, and has enabled various novel applications [3,4]. Motivated by its fundamental importance and potential applications, there have been efforts to study NDR in graphene [5–9], a prototypical two-dimensional material with tunable electronic properties [10–13]. However, tunneling-induced NDR has not yet been realized in graphene, while a recent study has proposed a new method for NDR in graphene that is not based on the quantum tunneling effect [9].

The scanning tunneling microscope (STM) is a powerful tool, which can not only directly probe NDR, but also provide key information on the mechanism. STM has been widely employed to study various electronic properties of graphene at the atomic scale, such as scattering and interference [14,15], but investigation into the subunit cell regime has been limited. Here, we report the first observation of NDR based on quantum tunneling at the vertical junction of STM over bilayer graphene. The applied electric field across bilayer graphene induces two van Hove singularities in the electronic spectrum, which are strongly localized on two sublattices in different layers. Such a localization of electronic singularities leads to a novel atomic-scale variation of NDR, which is directly visualized by our high-resolution tunneling spectroscopy within the

single unit cell of bilayer graphene. This result provides the atomic-level understanding of quantum tunneling in bilayer graphene.

Bilayer graphene was prepared on $6H$-SiC(0001) wafers (N-dopant concentration of 1×10^{18} cm^{-3}) by thermal graphitization in a flow of argon as described in Ref. [16]. The samples were transferred through the air to the ultrahigh vacuum chamber (5×10^{-11} torr), and briefly annealed up to 800 °C to refresh the surface. STM measurements were performed at 5.6 and 78.2 K using a commercial cryogenic STM (Unisoku, Japan), equipped with a Nanonis controller (Specs, Germany). dI/dV spectra were obtained by the standard lock-in technique with a modulation voltage of 3–18 mV at 500 Hz and a consistent set point of −0.2 V and 300 pA. The dI/dV map was taken by a grid spectroscopy, for which the thermal drift was carefully compensated by the atom-tracking method.

The basic configuration of our experimental setup is shown in Fig. 1(a). It involves the tunnel junction of an STM tip and bilayer graphene separated by a vacuum gap of about 1 nm. Using this technique we can measure I-V curves over a specific atomic site in the surface. The bilayer graphene is n doped with Fermi energy (E_F) about 0.3 eV above the charge-neutrality point [the Dirac energy (E_D)]. The interface of bilayer graphene with SiC(0001) produces a built-in electric field, rendering the charge densities in two stacked graphene layers inequivalent [17]. This out-of-plane symmetry breaking results in a band gap with the magnitude of 0.14 eV at E_D [11]. This characteristic of bilayer graphene has enabled a tunable band gap either by gating [12] or chemical doping [11], and is also important for NDR as explained below.
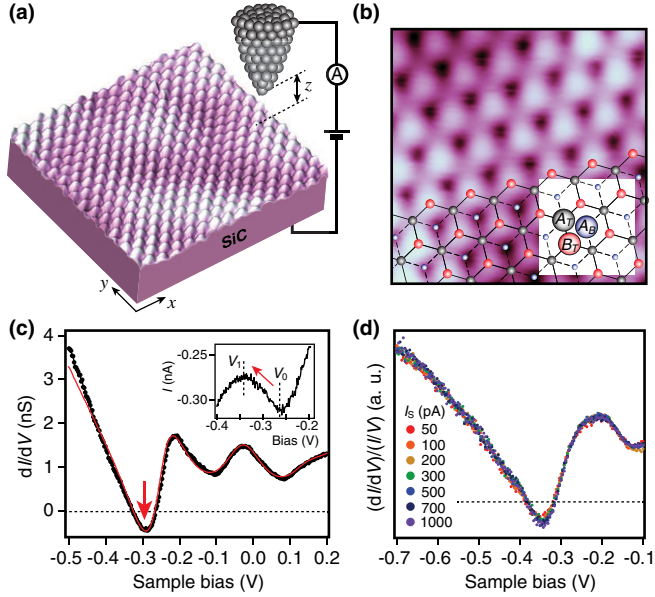
FIG. 1 (color online).   (a) Experimental configuration for the
local tunneling spectroscopy, consisting of an STM tip and
bilayer graphene on silicon carbide. (b) STM topographic image
$(1.5 \times 1.5$ nm$^2)$ taken on bilayer graphene with sample bias of
-0.2 V and tunneling current of 300 pA. Inset shows the atomic
structure overlaid with part of the STM image. Balls are carbon
atoms, and solid (dashed) lines represent chemical bonds in the
top (bottom) layer. (c) Point—dI/dV spectrum and a corre-
sponding I-V spectrum (inset) taken on the B_T site. The red
line overlaid is the result of model simulations. Red arrows
highlight NDR. (d) dI/dV spectra normalized by I-V at each
initial setting current marked. Dotted lines in (c) and (d) indicate
conductance zero.

Figure 1(b) shows an STM topographic image of bilayer
graphene, acquired with -0.2 V sample bias and constant
tunneling current. The atomic structure of bilayer graphene
is shown in the inset and overlaid with part of the image for
comparison. Bilayer graphene consists of two Bernal
stacked graphene layers, where the A sublattice of the
top layer (A_T, black) is located on the B sublattice of the
bottom layer (B_B). Due to the direct coupling between
them, the other sublattice in the top layer (B_T, red) is
dominantly imaged at low-bias voltage, resulting in the
triangular pattern [18,19]. The full honeycomb lattice
could be visualized at the higher bias voltage, confirming
the characteristic bias dependence of bilayer graphene
[20,21]. In Fig. 1(b), one can also readily distinguish the
A_T site from the hollow site in the top layer (corresponding
to A_B, blue) by their relative brightness. This demonstrates
the high spatial resolution achieved in our measurements.

Figure 1(c) shows a dI/dV curve measured on the B_T
site. The differential conductance value goes below zero at
-0.3 V, indicative of negative conductance (or resistance).
This can also be directly seen in I-V measurements [inset
of Fig. 1(c)] as decreasing current while increasing the
voltage from -0.26 to -0.34 V. This observation clearly

demonstrates NDR in bilayer graphene. The NDR behavior
was reproducibly observed in the voltage range of
$-0.30 \sim -0.35$ V, close to E_D. In Fig. 1(d), we display
a series of dI/dV spectra normalized by I/V taken with
different initial tunneling currents, which are inversely
related to the tip-sample distance (tunneling barrier width).
They show little change and consistent NDR behaviors,
excluding tip-induced origins of NDR such as a local band
bending [22].

An important clue for the origin of NDR can be obtained
from its spatial distribution at the atomic scale. Figure 2(a)
compares dI/dV curves on three different atomic sites
[refer to Fig. 1(b)]. NDR at -0.3 V occurs only on the
B_T site, while above $+0.1$ V the dominant conductance is
found on the A_T site. Recording dI/dV curves as a function
of lateral tip positions, we show a differential conductance
map at -0.3 V in Fig. 2(b). The simultaneously acquired
topographic image in the inset helps determine the atomic
position. Interestingly, negative conductance, represented
by blue color, is centered on each B_T atom and is sur-
rounded by a hexagonal rim of positive conductance. This
suggests that NDR is closely linked to localized states at
the B_T site. On the other hand, the same map taken at
$+0.17$ V shows dominant positive conductance on the A_T
site. This site-resolved detail has not been observed
previously most likely due to limited spatial resolution in
the tunneling spectroscopy. Indeed, the spatial average of
dI/dV curves [the black one in Fig. 2(a)] reproduces
the typical curve with no NDR reported previously in
literature [19].

To understand the origin of NDR, let us recall the
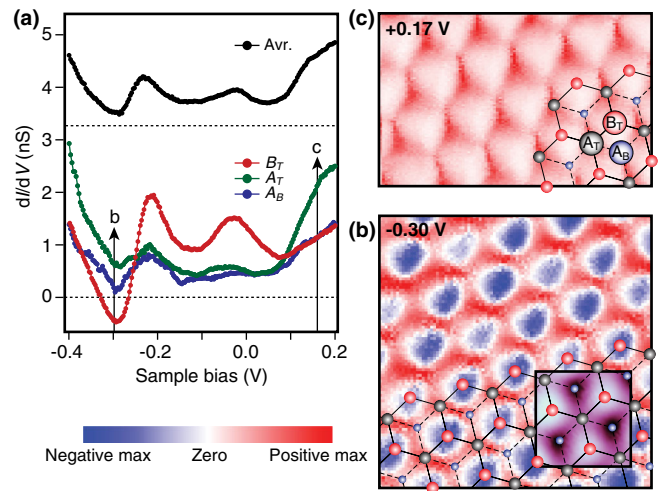band structure of bilayer graphene near E_F as illustrated

FIG. 2 (color online).   (a) Point—dI/dV spectra taken on
three different atomic sites of bilayer graphene, and its spatial
average offset for clarity. Dotted lines indicate conductance zero.
(b), (c) dI/dV maps taken with a 96×96 grid at the bias voltage
indicated by arrows in (a). The inset in (b) shows the simulta-
neously acquired topographic image overlaid with the atomic
structure of bilayer graphene.

in Fig. 3(a). In pristine bilayer graphene, there are two pairs of energy bands (dotted lines)—a low-energy pair from the B_T and A_B atoms and a high-energy pair from the A_T and B_B atoms. When a band gap is induced by a transverse electric field, the low-energy bands develop a Mexican-hat-like dispersion at conduction and valence band edges near the band gap [23,24]. This rather flat dispersion leads to two distinct van Hove singularities in the density of states [25] as in Fig. 3(b). Furthermore, these two near-gap states were theoretically predicted to be localized at specific atomic sites in different layers, as shown in Figs. 3(a) and 3(b), depending on the direction of the electric field [26,27]. Such a strong localization of electronic singularities (the flat parts of energy bands) is also important in understanding many-body correlations at low energies and the ground state of bilayer graphene [28], but has not been directly shown by experiments.
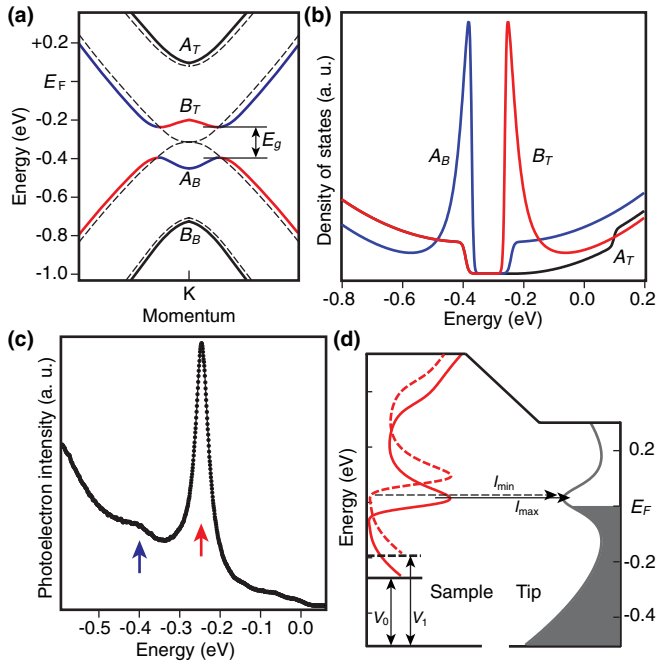

FIG. 3 (color online). (a) Band structure of bilayer graphene with (solid lines) and without (dashed lines) the band gap. Red and blue colors in a low-energy band pair represent the atomic site, at which corresponding states are localized (B_T: red, A_B: blue). (b) Site-resolved density of states in biased bilayer graphene [26,27]. (c) Energy-distribution curve at the K point taken by ARPES. Data were taken at the Advanced Light Source, using a Scienta R4000 electron analyzer (VG-Scienta, Sweden) and a 95-eV photon. Energy and angular resolutions were 30 meV and 0.1°. Red and blue arrows indicate positions of two van Hove singularities. (d) Energy diagram for the tunnel junction of the tip and the sample. Red solid and dashed lines are, respectively, the sample density of states at V_0 for local maximum current (I_{max}) and at V_1 for local minimum current (I_{min}) after broadening by Gaussian. The gray line is the tip density of states, and the shaded region is the filled tip states below E_F.

In our case, states near -0.25 and -0.39 eV are localized at B_T in the top layer (red) and at A_B in the bottom layer (blue), respectively, while states near $+0.1$ eV are localized at A_T in the top layer (black). Since STM is highly sensitive to the local density of states in the surface, this explains dominant conductance at B_T for $-0.2 \sim +0.1$ V in Fig. 2(a) and that at A_T above $+0.1$ V in Figs. 2(a) and 2(c). This picture is fully supported by the energy-distribution curve at the K point [Fig. 3(c)], measured by angle-resolved photoemission spectroscopy (ARPES). It reveals highly asymmetric intensities for the two van Hove singularities [11], because the photoelectrons excited from the bottom layer (A_B) are attenuated by scattering during their passage though the top layer. This also confirms that the layer localization is universal over the wide area covered by the photon beam (~ 50 μm in radius) in ARPES.

The presence of a layer-polarized van Hove singularity can qualitatively explain NDR, as in Fig. 3(d), which shows the relationship between the broadened sample density of states at B_T and the tip density of states. When the sample bias equals V_0, where the van Hove singularity meets the E_F of the tip, the current reaches a local maximum, I_{max}. As it approaches V_1, where the van Hove singularity no longer assists tunneling and no state exists in the band gap, tunneling is strongly suppressed, and the current decreases down to I_{min}. As the voltage further increases out of the band gap, the current starts increasing again, resulting in the N shaped branch in the I-V curve [as in the inset of Fig. 1(c)]. That is, the observed NDR is the result of electronic spectrum reconstructions in asymmetric bilayer graphene.

For the quantitive analysis, we performed I-V simulations based on the standard formula, $I(V, z) \propto \int_{E_F-V}^{E_F} \mathrm{DOS}_{sample}(E + V)\mathrm{DOS}_{tip}(E)T(E, V, z)dE$, where DOS is the density of states and T is the tunneling matrix element [29–31]. T is estimated by the WKB approximation as $T(E, V, z) = \exp(-2\sqrt{2(\phi - V/2 - E)}z)$, where ϕ is the work function. We used the Gaussian-broadened local DOS in the theoretical calculation [26,27] at B_T with a small contribution of that at A_T (to take into account the finite areal averaging). The tip DOS is assumed to have a typical localized state of tip-apex atoms near E_F [29]. The sample and tip DOS's optimized to reproduce the experimental data are presented, respectively, by red and gray curves in Fig. 3(d). The simulated curve [the red line overlaid in Fig. 1(c)] successfully reproduces the NDR behavior, confirming the proposed mechanism.

To further support the proposed mechanism, we have investigated the interaction of NDR with local defects. Recent theories predict that a single point scatterer in bilayer graphene develops in-gap states, suppressing the sharp van Hove singularities [32,33]. Thus, one might expect a local suppression of NDR near defects. Figure 4(a) shows a large scale STM image of an impurity (yellow blob).
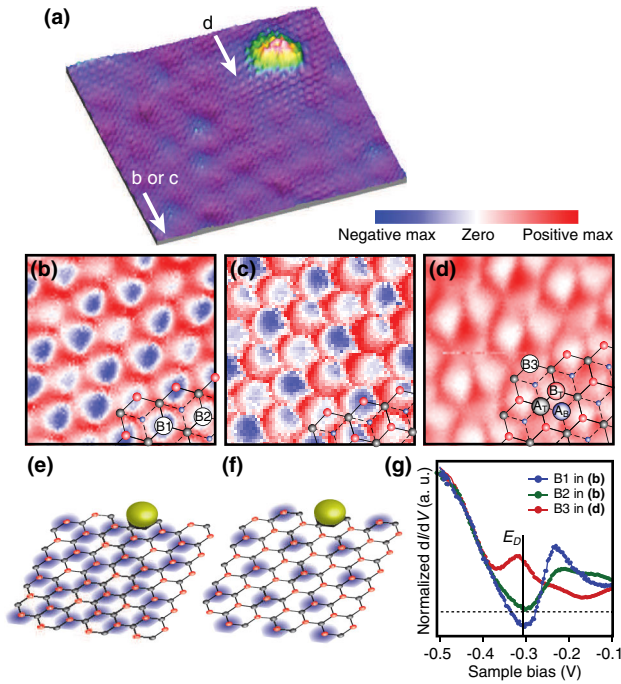
FIG. 4 (color online). (a) STM image (10×10 nm^2) with -0.05 V and 300 pA, where a local defect (the yellow blob) is present at the corner. dI/dV maps taken (b),(c) at two different regions about 16 nm away from defects and (d) at a region right next to a defect. The atomic structure of bilayer graphene is overlaid. (e),(f) Schematic illustration for two possible NDR patterns due to constructive or destructive interference of defect scatterings. (g) Normalized dI/dV spectra taken on three different B_T atoms marked in (b) and (d). Solid and dotted lines indicate E_D and conductance zero, respectively.

The dI/dV maps taken at two different locations about 16 nm away from defects are present in Figs. 4(b) and 4(c). NDR is extinguished in a subset of B_T atoms, which form a periodic $\sqrt{3} \times \sqrt{3}$ pattern rotated by 30° with respect to the lattice constant, and these data show little dependence on the origin and site of defects. The $(\sqrt{3} \times \sqrt{3})R30°$ modulation is the well-known signature of intervalley electron scattering by a defect in bilayer graphene [14,15]. Thus, we attribute two inverse patterns in Figs. 4(b) and 4(c) to constructive or destructive interference of defect scattering, as illustrated in Figs. 4(e) and 4(f). Furthermore, the same map taken right next to a defect [Fig. 4(d)] shows that NDR completely disappears and instead strong positive conductance emerges on a subset of B_T atoms. As a result, positive, zero, and negative conductance are all possible [solid line in Fig. 4(g)], and defects can be used to switch NDR on and off nearby as well as at the site more than 10 nm away from a defect. Such a strong impact of defects in electronic localization should be considered for the complete understanding of scattering and interference in bilayer graphene [14,15]. The disappearance of NDR with the progressive suppression of the van Hove singularity near the band gap [the peak at -0.23 V in

Fig. 4(g)] makes a clear link between them. This will further allow the control of NDR by tuning the band gap with gating or chemical doping [11,12].

Our results, combined with a few existing techniques, suggest a route towards graphene-based NDR devices. The key to NDR is, as demonstrated here, to exploit the near-gap van Hove singularity in biased bilayer graphene. In our experimental configuration, the tip can be replaced by another biased bilayer graphene, such that a vertical tunnel junction of two graphene bilayers is formed. A similar graphene heterostructure has recently been realized using ultrathin boron nitride films as a tunneling barrier [1,2]. In such junctions, tunneling would depend on sublattice-registry matching. That is, if the sublattices in two graphene layers facing each other, where the van Hove singularity is localized, were to line up, maximal direct tunneling between van Hove singularities could be achieved. The tunable electronic structure of bilayer graphene [11,34,35] would allow further optimization for NDR and a large peak-to-valley ratio of tunneling current.

*yeom@postech.ac.kr
†abostwick@lbl.gov

[1] L. Britnell *et al.*, Science **335**, 947 (2012).
[2] L. Britnell *et al.*, Nano Lett. **12**, 1707 (2012).
[3] L. Esaki, Phys. Rev. **109**, 603 (1958).
[4] L. L. Chang, L. Esaki, and R. Tsu, Appl. Phys. Lett. **24**, 593 (1974).
[5] R. Nandkishore and L. Levitov, Proc. Natl. Acad. Sci. U.S.A. **108**, 14 021 (2011).
[6] G. Fiori, IEEE Electron Device Lett. **32**, 1334 (2011).
[7] Z. F. Wang, Q. Li, Q. W. Shi, X. Wang, J. Yang, J. G. Hou, and J. Chen, Appl. Phys. Lett. **92**, 133114 (2008).
[8] K. M. Masum Habib, F. Zahid, and R. K. Lake, Appl. Phys. Lett. **98**, 192112 (2011).
[9] Y. Wu, D. B. Farmer, W. Zhu, S.-J. Han, C. D. Dimitrakopoulos, A. A. Bol, P. Avouris, and Y.-M. Lin, ACS Nano **6**, 2610 (2012).

[10] A. K. Geim and K. S. Novoselov, Nat. Mater. **6,** 183 (2007).

[11] T. Ohta, A. Bostwick, T. Seyller, K. Horn, and E. Rotenberg, Science **313,** 951 (2006).

[12] Y. Zhang, T.-T. Tang, C. Girit, Z. Hao, M. C. Martin, A. Zettl, M. F. Crommie, Y. Ron Shen, and F. Wang, Nature (London) **459,** 820 (2009).

[13] Y.-M. Lin, C. Dimitrakopoulos, K. A. Jenkins, D. B. Farmer, H.-Y. Chiu, A. Grill, and Ph. Avouris, Science **327,** 662 (2010).

[14] G. M. Rutter, J. N. Crain, N. P. Guisinger, T. Li, P. N. First, and J. A. Stroscio, Science **317,** 219 (2007).

[15] I. Brihuega, P. Mallet, C. Bena, S. Bose, C. Michaelis, L. Vitali, F. Varchon, L. Magaud, K. Kern, and J. Y. Veuillen, Phys. Rev. Lett. **101,** 206802 (2008).

[16] K. V. Emtsev *et al.*, Nat. Mater. **8,** 203 (2009).

[17] S. Kopylov, A. Tzalenchuk, S. Kubatkin, and V. I. Fal'ko, Appl. Phys. Lett. **97,** 112109 (2010).

[18] J. Tersoff and N. D. Lang, Phys. Rev. Lett. **65,** 1132 (1990).

[19] P. Lauffer, K. V. Emtsev, R. Graupner, Th. Seyller, L. Ley, S. A. Reshanov, and H. B. Weber, Phys. Rev. B **77,** 155426 (2008).

[20] G. M. Rutter, J. N. Crain, N. P. Guisinger, P. N. First, and J. A. Stroscio, J. Vac. Sci. Technol. A **26,** 938 (2008).

[21] See Supplemental Material at http://link.aps.org/supplemental/10.1103/PhysRevLett.110.036804 for the bias dependence of STM images.

[22] W. Jung, D. Cho, M.-K. Kim, H.-J. Choi, and I.-W. Lyo, Proc. Natl. Acad. Sci. U.S.A. **108,** 13 973 (2011).

[23] E. McCann and V. I. Fal'ko, Phys. Rev. B **96,** 086805 (2006).

[24] H. Min, B. Sahu, S. K. Banerjee, and A. H. MacDonald, Phys. Rev. B **75,** 155115 (2007).

[25] F. Guinea, A. H. Castro Neto, and N. M. R. Peres, Phys. Rev. B **73,** 245426 (2006).

[26] E. K. Yu, D. A. Stewart, and S. Tiwari, Phys. Rev. B **77,** 195406 (2008).

[27] A. Ramasubramaniam, D. Naveh, and E. Towe, Nano Lett. **11,** 1070 (2011).

[28] J. Velasco, Jr *et al.*, Nat. Nanotechnol. **7,** 156 (2012).

[29] I.-W. Lyo and P. Avouris, Science **245,** 1369 (1989).

[30] M. Grobis, A. Wachowiak, R. Yamachika, and M. F. Crommie, Appl. Phys. Lett. **86,** 204102 (2005).

[31] B. W. Heinrich, M. V. Rastei, D.-J. Choi, T. Frederiksen, and L. Limot, Phys. Rev. Lett. **107,** 246801 (2011).

[32] J. Nilsson and A. H. Castro Neto, Phys. Rev. Lett. **98,** 126801 (2007).

[33] F. M. D. Pellegrino, G. G. N. Angilella, and R. Pucci, Phys. Rev. B **80,** 094203 (2009).

[34] G. Li, A. Luican, J. M. B. Lopes dos Santos, A. H. Castro Neto, A. Reina, J. Kong, and E. Y. Andrei, Nat. Phys. **6,** 109 (2010).

[35] S.-M. Choi, S.-H. Jhi, and Y.-W. Son, Nano Lett. **10,** 3486 (2010).